

Iron line profiles from black hole accretion discs with spiral velocity structure

Sean A. Hartnoll¹ and Eric G. Blackman²

¹ *DAMTP, Centre for Mathematical Sciences, Wilberforce Road, Cambridge CB3 0WA, UK.*

² *Department of Physics & Astronomy, and Laboratory for Laser Energetics, University of Rochester, Rochester NY 14627, USA.*

Submitted version

ABSTRACT

We calculate the iron line profiles from accretion discs with spiral velocity structures around Schwarzschild black holes. We find that quasi-periodic bumps appear in the the profiles, thereby providing a test for spiral wave patterns. This study is motivated by recent work showing that spiral density waves can result from MHD instabilities even in non-self-gravitating discs, and by improved spectral resolution of forthcoming X-ray missions.

Key words: accretion, accretion disc - instabilities - line: formation - line: profiles - galaxies: active - X-rays: galaxies

1 INTRODUCTION

Active galactic nuclei (AGN) and some X-ray binaries are thought to be powered by accretion onto a central black hole (e.g. Rees 1984). A fluorescent iron $K\alpha$ emission line with rest energy 6.4 keV is observed in the X-ray spectrum of many Seyfert galaxies and some X-ray binaries. The line profile is shaped by Döppler and gravitational redshifts (Fabian *et al.* 1989) and therefore by the geometry and dynamics in the innermost regions of the accretion engine (e.g. Fabian *et al.* 2000 for a review).

The simplest plausible geometry to explain the observed profiles is a geometrically thin, optically thick disc with an X-ray corona above and below the disc. Some of the X-rays emanate directly to the observer, and others are reprocessed by the disc, inducing the iron line. General relativity is needed to calculate the redshifts and photon trajectories. This has been done for both Schwarzschild (Fabian *et al.* 1989) and Kerr (Laor 1991) black holes. The resulting profiles have been successful in reproducing many features of the experimental data (e.g. Tanaka *et al.* 1995; Nandra *et al.* 1997).

The primary motivation for the present work is that MHD instabilities can induce spiral density waves in non-self-gravitating accretion discs (Caunt and Tagger 2001, Hawley 2001, Tagger and Pellat 1999). It is therefore interesting to see whether this spiral structure has a significant effect on iron line profiles.

The effect of spiral structure on line profiles has been considered before in the context of tidally induced spiral shocks in close binary systems (e.g. Chakrabarti and Wiita 1993, Steeghs and Stehle 1999). The non-axisymmetry of the situation was emphasised by Sanbuichi, Fukue and Kojima

(1994), who also considered special relativistic effects. For a review of numerical work on spiral shocks in close binaries see Matsuda *et al.* (2000).

This work differs from previous considerations of spiral structure because the context is iron lines from AGN and therefore we use general relativity. For non-self-gravitating discs, and discs not in binaries, spiral structure is still possible, but requires MHD instabilities (Caunt and Tagger 2001, Hawley 2001, Tagger and Pellat 1999). The changes to the profile come purely from the spiral *velocity* structure and the corresponding modified redshifts.

We find that the spiral velocity structure does have a significant effect on the profiles. Most notably by introducing multiple quasi-periodic sub-peaks into the profile, particularly visible for tightly packed spirals. For reasonable values for the parameters of the spiral structure, the effects on the line profiles require better spectral resolution than is currently available (e.g. Nandra *et al.* 1997), but will likely be discernable with Astro E-2. We can therefore make predictions.

Like warping (see Bachev 1999, Hartnoll and Blackman 2000) spiral structure induces non-axisymmetric effects on the line profiles, though the tighter the winding of the spiral the less the observed effect. Nevertheless, one immediate effect of non-axisymmetry is a time dependence in the line profile of rotating discs. Spiral shocks were used in this way by Chakrabarti and Wiita (1994) to study variable broad optical emission lines in AGN. In fact a time dependence in the iron X-ray line is also observed (e.g. Iwasawa *et al.* 1996) and has been argued to be problematic for the standard disc models (e.g. Weaver and Yaqoob 1998, Sulentic *et al.* 1998). Although the issue remains unresolved, some kind of non-axisymmetry of the disc may be playing a role.

It is straightforward to adapt the standard calculations of line profiles to include spiral structure. The main difference is that the azimuthal velocity of the gas is no longer Keplerian and the radial velocity is nonzero. Representative expressions for the azimuthal and radial velocities are given in §2. In §3 we list the formulae needed to compute the profiles, in order that our paper be self-contained. In particular the redshift formula needs to be generalised for non-Keplerian rotation. §4 contains sample profiles and explanation of the new features. §5 contains a discussion of the results.

2 SPIRAL WAVES IN ACCRETION DISCS

We use a simple representation of spiral structure in the gas velocity, motivated by the numerical results of Caunt and Tagger (2001)

$$v_r = r^{-1/2} \epsilon_r e^{-(r-r_{in})/r_0} \cos(m\phi - kr), \quad (1)$$

$$v_\phi = r^{-1/2} \left(1 + \epsilon_\phi e^{-(r-r_{in})/r_0} \cos(m\phi - kr + \Delta) \right), \quad (2)$$

where r_0 is a constant parametrising the fall-off with radius r , m is the azimuthal wavenumber, k is larger for more tightly packed spirals, ϵ is the size of the perturbation, Δ allows the velocities to be out of phase. So $(\epsilon_r, \epsilon_\phi, m, k, r_0, \Delta)$ is the parameter space of discs. We then combine these with the angle of disc inclination to the observer, and the azimuthal viewing angle of the observer. See Fig. 1 for an example disc. Note that in this work we consider spiral waves which are stationary over the observation duration. There could in addition be a time dependent phase in eqs. (1) and (2) to account for a rapid spiral wave propagation.

3 CALCULATION OF THE LINE PROFILE

3.1 Total flux

The total flux observed at frequency ν is given by

$$F(\nu) \propto \int \delta(\nu - \nu_0(\mathbf{r})) f(\mathbf{r}, \nu) d^2x, \quad (3)$$

where the integral is over the disc, $\nu_0(\mathbf{r})$ is the observed frequency of flux emitted from \mathbf{r} and $f(\mathbf{r}, \nu)$ is given by

$$f(\mathbf{r}, \nu) = \left[\frac{\nu}{\nu_e} \right]^3 f_{out}(\mathbf{r}, \hat{\mathbf{c}}(\mathbf{r}, \hat{\mathbf{n}})), \quad (4)$$

where $\left[\frac{\nu}{\nu_e} \right]^3$ is the relativistic correction to the flux, with the frequency of emission, $\nu_e = 6.4\text{keV}$ for the fluorescent iron line. The function $f_{out}(\mathbf{r}, \hat{\mathbf{c}})$ is the flux reprocessed and re-emitted at \mathbf{r} in the direction $\hat{\mathbf{c}}$, defined such that emitted photons in this direction from the disc eventually reach the observer in the Schwarzschild metric. The asymptotic direction to the observer is $\hat{\mathbf{n}}$.

The range of emitting region we consider is $6 = r_{in} \leq r \leq r_{out} = 60$ and $0 \leq \phi < 2\pi$, in units with $c = G = M = 1$. The lower bound is the innermost stable orbit of the Schwarzschild metric and the upper bound is somewhat arbitrary, but unimportant, as the objective is to compare our results here with profiles from discs with axisymmetric density structures that have well known dependences on outer radius (e.g. Fabian *et al.* 1989). Moreover, most of the

interesting effects will occur in the inner regions. The area element has a general relativistic correction, so

$$d^2x = \frac{dr}{\sqrt{1 - \frac{2}{r}}} r dr d\phi. \quad (5)$$

3.2 Photon paths: direction of emission

We use paths in the Schwarzschild metric, approximated by a first order perturbation. In this approximation, the initial direction $\hat{\mathbf{c}}$ of the photon at \mathbf{r} reaching the observer, (i.e. in asymptotic direction $\hat{\mathbf{n}}$) is (Hartnoll and Blackman 2001)

$$\mathbf{c}(\mathbf{r}) = -\frac{d\mathbf{r}_{ph}}{d\Phi} (\Phi = \Phi_0), \quad (6)$$

where Φ parametrises the photon path and

$$\mathbf{r}_{ph}(\Phi) = r_{ph}(\Phi) \left[\cos \Phi \hat{\mathbf{n}} + \sin \Phi \frac{\mathbf{r} - (\mathbf{r} \cdot \hat{\mathbf{n}}) \hat{\mathbf{n}}}{r} \right] \quad (7)$$

and the initial value Φ_0 is given by

$$\cos \Phi_0 = \frac{\mathbf{r} \cdot \hat{\mathbf{n}}}{r}, \quad (8)$$

with $\Phi_0 \in [0, \pi]$. Further $r_{ph}(\Phi)$ is

$$\frac{1}{r_{ph}(\Phi)} = \frac{\sin \Phi}{2R} + \frac{1 + C \cos \Phi + \cos^2 \Phi}{4R^2} + \mathcal{O}\left(\frac{1}{R^3}\right), \quad (9)$$

where

$$C = -2, \quad (10)$$

$$R = \frac{r \sin \Phi_0}{4} + \frac{r}{4} \sqrt{\sin^2 \Phi_0 + \frac{4}{r} (1 - \cos \Phi_0)^2}. \quad (11)$$

This perturbative approach is valid throughout most of the disc and sufficient for our purposes. Corrections to the photon paths due to strong curvature in the innermost regions are most significant for very high inclination angle profiles (Matt, Perola and Stella 1993).

3.3 Frequency shifts

The observed frequency of radiation from \mathbf{r} in the Schwarzschild metric is (e.g. Hartnoll and Blackman 2001)

$$\nu_0(\mathbf{r}) = \frac{\nu_e \sqrt{1 - \frac{2}{r} - \frac{u_r^2(\mathbf{r})}{1 - \frac{2}{r}} - u_\phi^2(\mathbf{r})}}{1 - \frac{\hat{c}_r(\mathbf{r}) \hat{c}_r(\mathbf{r})}{1 - \frac{2}{r}} - \hat{c}_\phi(\mathbf{r}) u_\phi(\mathbf{r})}. \quad (12)$$

Here $\mathbf{u}(\mathbf{r})$ is the velocity of the emitting material at \mathbf{r} , given in the previous section. As noted in Hartnoll and Blackman (2001), in this context $\hat{\mathbf{c}}$ needs to be normalised so that $\frac{\hat{c}_r(\mathbf{r}) \hat{c}_r(\mathbf{r})}{1 - \frac{2}{r}} + \hat{c}_\theta(\mathbf{r}) \hat{c}_\theta(\mathbf{r}) + \hat{c}_\phi(\mathbf{r}) \hat{c}_\phi(\mathbf{r}) = \frac{1}{1 - \frac{2}{r}}$. Fig. 2 shows the redshifts for a sample disc.

3.4 Reprocessed flux

We need to calculate $f_{out}(\mathbf{r}, \hat{\mathbf{c}})$. We use the standard iron line model (Fabian *et al.* 1989) in which there is assumed to be a corona above the central region producing hard X-rays which are reprocessed by the disc. The corona is modelled by a source which is at height h_s directly above the centre of the disc. So the flux impinging on the disc at \mathbf{r} is

$$f_{in}(\mathbf{r}) \propto \frac{h_s}{(h_s^2 + r^2)^{q/2}}. \quad (13)$$

We will take $q = 3$ (i.e. $1/r^2$ falloff from source) and $h_e = 10$. The main objective is to study the effect of spatial inhomogeneity on the line profiles, so the exact values of these parameters are not important so long as they allow us to compare the results with standard line profiles. Assuming the re-emission is isotropic, we have

$$f_{out}(\mathbf{r}, \hat{\mathbf{c}}) \propto f_{in}(\mathbf{r}) \mathbf{e}_z \cdot \hat{\mathbf{c}}, \quad (14)$$

where \mathbf{e}_z is the unit normal to the disc. Note that the varying density will affect the optical depth but not the total power coming from a given radius as long as the optical depth is $\gg 1$. We do not incorporate the vertical density structure of the disc in calculating our line profiles.

4 DISCUSSION OF LINE PROFILES

The region of the parameter space investigated in this section is qualitatively guided by recent numerical results from simulations of spiral structure in non-self-gravitating MHD accretion discs (Caunt and Tagger 2001, Hawley 2001).

Fig. 3 shows profiles from discs at 30 degrees inclination for various values of k and r_0 . The spiral velocity structure results in the presence of small peaks across the profile. As expected, increasing k increases the frequency of the peaks. At lower r_0 , the spiral structure is more confined to the inner regions. Note that $\epsilon = \epsilon_r = \epsilon_\phi$ needs to be changed with r_0 to ensure that the overall normalisation is comparable. A concentration of structure at small r reveals itself through the prevalence of peaks or bumps appearing in the more redshifted or blueshifted regions of the profile.

Fig. 4 shows profiles from discs at 15 degrees inclination for various k and a profile with no spiral structure for comparison. A larger range of k is considered in comparison to Fig. 3. Again the correlation between number of peaks and k is evident.

Fig. 5 shows profiles from discs at an inclination angle of 60 degrees. The profiles from discs at high inclination angles are naturally more spread out. The effects of k and r_0 are as before. It is particularly noticeable in these profiles that the sub-peaks occur only outside of the standard double peaks. This is due to the falloff with r ; the spirals are more prominent in the inner regions of the disc, which are more Doppler shifted. The atypical blueshifted region of the $k = 1.2$, $r_0 = 15$ graph is also interesting, the sub-peaks evolve into a step-like form.

All discs considered above have $m = 1$, $\Delta = 0$, $\epsilon_r = \epsilon_\phi$ fixed given r_0 , and the observer is at the same azimuthal angle in all cases. Varying ϵ with r_0 fixed has the obvious effect of increasing the relative magnitude of the perturbations to the usual line profile from discs without spiral structure. Varying m , Δ or the azimuthal angle of the observer does not appear to have a significant qualitative effect on the profiles.

5 CONCLUSION

The most interesting overall feature in our line profiles is the presence of multiple, quasi-periodic sub-peaks in the most

red or blue-shifted regions, indicating spiral structure in the inner disc. The profiles can be compared with data to infer a constraint on dynamical models predicting spiral structure. Figs. 3, 4 and 5 show what sort of values of ϵ , for a given r_0 , are consistent with present data.

Though not easily constrained with current instruments, this quasi-periodic bumpiness should be resolvable with Astro E-2, which carries the X-ray Spectrometer (XRS) of spectral resolution $\Delta E/E \sim 0.002$ in the 6.4keV range (Kelley *et al.* 1999) which should be sufficient for a wide range of k . For very low k , there are fewer sub-peaks, and their exact shape and position depend on the variables m , Δ , $\frac{\epsilon_r}{\epsilon_\phi}$ and the azimuthal angle of the observer.

ACKNOWLEDGEMENTS

EGB acknowledges partial support from DOE grant DE-FG02-00ER54600.

REFERENCES

- Bachev R., 1999, A&A, 348, 71
 Caunt S.E. & Tagger M., 2001, A&A, 367, 1095
 Chakrabarti S.K. & Wiita P.J., 1993, A&A, 271, 216
 Chakrabarti S.K. & Wiita P.J., 1994, ApJ, 434, 518
 Fabian A.C., Rees M.J., Stella L. & White N.E., 1989, MNRAS, 238, 729
 Fabian A.C., Iwasawa K., Reynolds C.S. & Young A.J., 2000, PASP, 112, 1145.
 Hartnoll S.A. & Blackman E.G., 2000, MNRAS, 317, 880
 Hartnoll S.A. & Blackman E.G., 2001, MNRAS, 324, 257
 Hawley J.F., 2001, ApJ, 554, 534
 Iwasawa K., *et al.*, 1996, MNRAS, 282, 1038
 Kelley R.L. *et al.* 1999, Proc. SPIE, 3765, 114
 Laor A., 1991, ApJ, 376, 90
 Matsuda T., Makita M., Fujiwara H., Nagae T., Haraguchi K., Hayashi E., Boffin H.M.J, 2000, Ap&SS, 274, 259
 Matt G., Perola G.C. & Stella L., 1993, A&A, 267, 643
 Nandra K., George R.F., Mushotzky R.F., Turner T.J. & Yaqoob T., 1997, ApJ, 477, 602
 Rees M.J., 1984, ARA&A, 22, 417
 Sanbuichi K., Fukue J., Kojima Y., 1994, PASJ, 46, 605
 Steeghs D., Stehle R., 1999, MNRAS, 307, 99
 Sulentic J.W., Marziani P., Calvani M., 1998, ApJ, 497, L65
 Tagger M. & Pellat R., 1999, A&A, 349, 1003
 Tanaka Y. *et al.*, 1995, Nature, 375, 659
 Weaver K.A. & Yaqoo T., 1998, ApJ, 502, L139

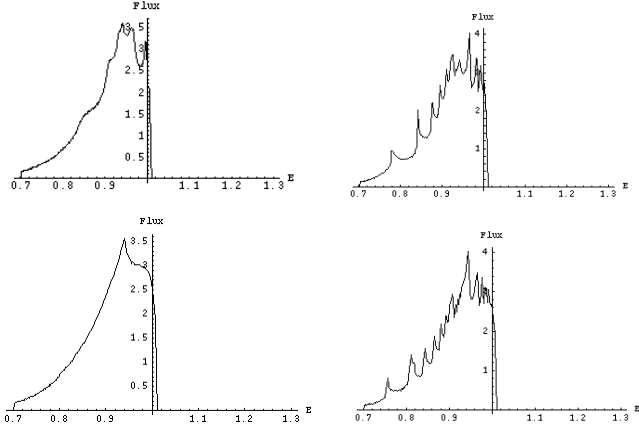


Figure 4: Clockwise from top left: The first three are profiles from discs at inclination angle 15 degrees with $m = 1$, $\Delta = 0$, $r_0 = 15, \epsilon = 0.2$. From left to right: $k = 0.4$, $k = 1.2$, $k = 2.0$. The profile at the bottom left is from a disc with no spiral structure, for comparison.

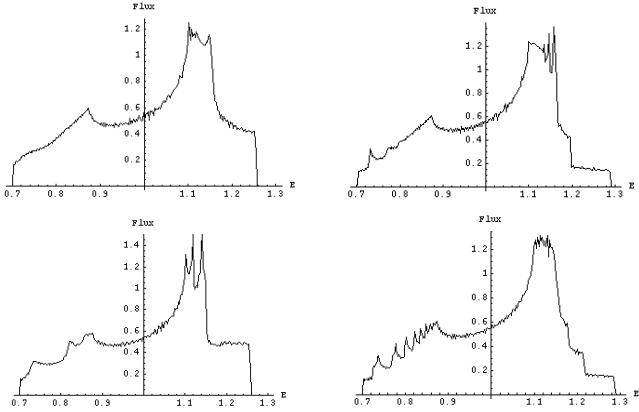


Figure 5: As for Fig. 3 but at inclination angle of 60 degrees. Left column: $k = 0.4$. Right column: $k = 1.2$. Top row: $r_0 = 5, \epsilon = 0.3$. Bottom row: $r_0 = 15, \epsilon = 0.2$.

Figure 1: The spiral structure of the radial velocity in a disc with $m = 1$, $k = 1.2$, $r_0 = 15$.

Figure 2: The redshifts of the disc of Fig. 1, viewed at an inclination angle of 30 degrees. Darker shading indicates higher redshift. The disc is rotating anticlockwise, the observer is situated to the right.

Figure 3: Profiles from discs at inclination angle 30 degrees with $m = 1$, $\Delta = 0$. Left column: $k = 0.4$. Right column: $k = 1.2$. Top row: $r_0 = 5, \epsilon = 0.3$. Bottom row: $r_0 = 15, \epsilon = 0.2$.

This figure "fig1.jpg" is available in "jpg" format from:

<http://arxiv.org/ps/astro-ph/0109243v1>

This figure "fig2.jpg" is available in "jpg" format from:

<http://arxiv.org/ps/astro-ph/0109243v1>

This figure "fig3.jpg" is available in "jpg" format from:

<http://arxiv.org/ps/astro-ph/0109243v1>